Supporting Information on:

The Solubility Advantage of Amorphous Ketoprofen. Thermodynamic and Kinetic Aspects by Molecular Dynamics and Free Energy Approaches

D. Gobbo,[(1)] P. Ballone,[(1,2,3)] S. Decherchi,[(1)] and A. Cavalli[(1,4)]

(1) Computational and Chemical Biology,

Fondazione Istituto Italiano di Tecnologia, Genova, Italy

(2) School of Physics, University College, Dublin, Ireland

(3) Conway Institute for Biomolecular and Biomedical Research,

University College, Dublin, Ireland and

(4) University of Bologna, Bologna, Italy

I. COMPUTATIONAL SETUP

Because of the variety and complexity of the computations, details and parameters defining the computational set-up are listed where they are actually used, and therefore they are spread in different subsections of Results. To ease the reproducibility of our computations, we summarise here all these parameters. The most crucial among them are reported here and in the main text.

Molecular dynamics The majority of the computations is represented by molecular dynamics simulations (MD), based on the GAFF force field[1] for KTP, and on the SPC/Fw[2] force field for water. The GAFF potential energy of the KTP molecule has been shifted upwards by 20.83 kJ/mol in such a way that its ground state energy vanishes. In a similar way, the computed free energy of neutral (undissociated) KTP in solution is shifted downwards by $\Delta F = 23.58$ kJ/mol to account for the acidic dissociation of KTP in water at low concentration (pH= 7), according to the results of Ref. 22, 35.

MD simulations have been used to compute absolute free energies, and to qualitatively characterise the kinetics of KTP dissolution in water. These two stages have been carried out using different but equivalent packages and set-ups.

MD simulations required to compute absolute free energies are carried out in the NVT ensemble using the velocity Verlet algorithm with a time step of 1 fs. Constant temperature has been enforced by a Langevin thermostat[3] with a relaxation time of 10 ps. Periodic boundary conditions are applied to all condensed phases, i.e., with the exception of the computations for the gas-phase KTP molecule to compute the vapour pressure in equilibrium with c-KTP. Since at this stage our samples are relatively small, Coulomb interactions are accounted for using the Ewald sum, with a real space cut-off of 10 Å and a reciprocal space cut-off $G^2_{cut} = 3.8^2$ Å $^{-2}$.

A. The QH computations

The QH computations are started from a configuration of local energy minimum found by quenching a sample equilibrated at $T = 300$K. The quench is not sudden, but it consists of discrete temperature drops (by velocity rescaling) of 50 K from $T = 300$ K down to 150 K. Each drop is followed by 5 ps of local equilibration. Below $T = 150$ K the energy

minimisation proceeds by quenched MD, in which velocities are set to zero whenever $\sum_i \mathbf{F}_i \cdot \mathbf{v}_i < 0$, where $\mathbf{F}_i$ and $\mathbf{v}_i$ are the force and the velocity of particle i, respectively.

The second derivatives of the potential energy entering the determination of the dynamical matrix $D_{ij}^{\alpha\beta}$ have been computed by finite differences, displacing coordinates by 0.05 Å in every direction.

As stated in the main text, the harmonic free energy F_h of Eq. (4) is an implicit function of the system volume, whose minimisation at any given T gives the equilibrium volume.

The experience of practical computations shows that the harmonic free energy as a function of the system volume is somewhat rugged, especially for small systems and for hydrogen-bonded materials. To remove the effect of minor energy variations in the determination of the volume of minimum free energy, a smooth interpolation is often used, relying on semi-empirical expressions, such as the Birch-Murnaghan equation of state:[4]

$$P(V) = -\left(\frac{\partial F}{\partial V}\right)_{T,N} = \frac{3B_0}{2}\left[\left(\frac{V_0}{V}\right)^{7/3} - \left(\frac{V_0}{V}\right)^{5/3}\right]\left\{1 + \frac{3}{4}(B' - 4)\left[\left(\frac{V_0}{V}\right)^{2/3} - 1\right]\right\} \quad (1)$$

where P is the pressure, V is the volume, V_0 is the equilibrium volume at $P = 0$, B_0 is the bulk modulus at $P = 0$, B' is the pressure derivative of the bulk modulus, again at $P = 0$. Strictly speaking, the expression in Eq. 1 is suitable for cubic systems, but this is not a limitation for amorphous and liquid systems. In practice, the QH equation of state has been determined by interpolating the volume-dependent harmonic results covering a range of $0.94V_{ref} \leq V \leq 1.07V_{ref}$, where V_{ref} is a reference volume corresponding to the density $\rho = 1.0$ g/cm^3. The harmonic free energy F_{QH} at the optimal volume V_{QH} determined in this way is the QH free energy of the system at $T = 300$ K.

B. The λ- and β-integration

The integration over λ introduced by Eq. 5 of the main text:

$$\Delta F_\lambda(V, T, N) = \int_0^1 \langle \Delta U[\{\mathbf{R_i}, i = 1, ..., N\}]\rangle_\lambda d\lambda \quad (5)$$

has been limited to $0 \leq \lambda \leq 0.995$, and computed by the trapezoidal rule over the points: $\lambda = 0$ (harmonic); 0.005; 0.01; 0.05; 0.1; 0.2; ...; 0.9; 0.95; 0.99; 0.9925; 0.995. Up to $\lambda = 0.9$, averaging has been carried out over 0.7 ns; beyond $\lambda = 0.9$, averaging has been progressively

extended, reaching 8 ns at $\lambda = 0.995$. Also equilibration time has been increase from 1 ns at low λ up to 12 ns at $\lambda = 0.995$.

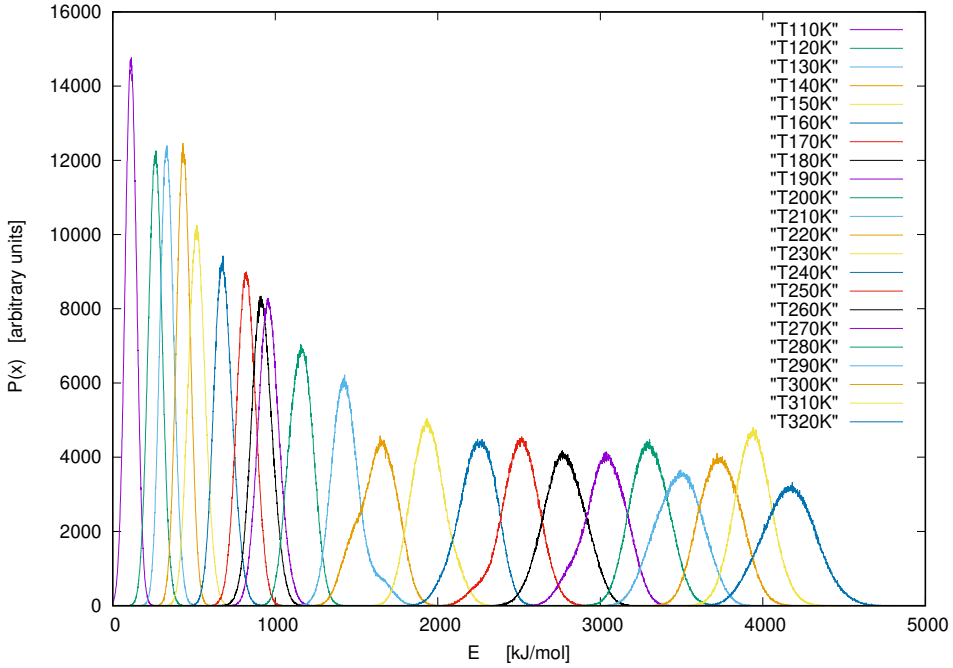

FIG. S1: Probability distribution of energies over the 22 temperature windows spanning the $110 \leq T \leq 320$ K range, used to carry out the TI over the inverse temperature β (see text). Probabilities are unnormalised, but all curves cover the same area. Energies refer to the entire sample made of one KTP and $N_w = 300$ water molecules, measured from a common shifted origin.

The integration over β (Eq. (8) of the main text) covered the interval $100 \leq T \leq 300$, using data collected every 10 K from $T = 100$K to $T = 320$ K. At each temperature, averaging covered 1.3 ns following 2.8 ns equilibration. The overlap of the potential energy distribution from the fixed temperature runs are shown in Fig. S1.

C. Steered MD (sMD) and umbrella sampling (US)

All MD simulations required to characterise the kinetics of KTP dissolution in water were performed using GROMACS version 2016.5.[5] Short-range electrostatic interactions were treated with the Verlet cut-off scheme[6] and long-range ones with the Particle Mesh Ewald (PME)[7] method. In both cases, the cut-off was fixed at 1 nm. Periodic boundary conditions (PBC) were applied. At the beginning, the steepest descent algorithm was chosen to energy

minimize the system. For all MD simulations, Langevin dynamics[3] with a time constant for coupling equal to 2.0 ps was used. For simulations performed in the NPT ensemble, the average pressure of the system was equilibrated to 1 atm according to Parrinello-Rahman barostat.[8] The integration time step was set to 1 fs because of application of the flexible 3-points water model.

Two putative solvation paths of KTP in the glass and crystal forms were generated by steered molecular dynamics (sMD).[9] To this aim, a pulling force with a force constant of 2000 kJ mol^{-1} nm^{-2} was imposed on the centre of mass (COM) of one of the KTP molecules located at the solid/water interface and directed towards the solvent. The rate of change of the reference position was fixed at 0.1 nm ns^{-1}.

The harmonic force constant applied to the selected umbrella sampling windows was set equal to 1000 kJ mol^{-1} nm^{-2}. To improve the sampling of the transition state of the dissolution paths, the force constant was increased up to 4000 kJ mol^{-1} nm^{-2}.

The free energy profile (potential of mean force) along a single reaction coordinate corresponding to the transfer of one ketoprofen molecule from the crystal or amorphous solid to the solution has been computed by using the so-called weighted histogram analysis method (WHAM).[10] A check of the result has been carried out by reconstructing the same profile using a different method, known as the umbrella integration (UI) approach.[11–13]

The overlap of density histograms used to reconstruct the free energy profiles, the comparison of results from closely related methods, and the estimation of error bars on the free energy profiles are shown in Fig. S2, Fig. S3, Fig. S4, Fig. S5.

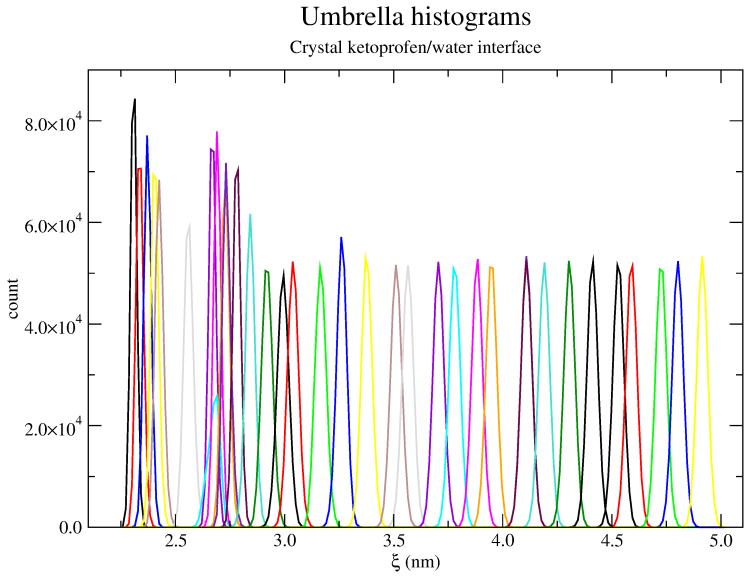

FIG. S2: Overlap of histograms used to reconstruct the free energy profile (see text) in the c-KTP case

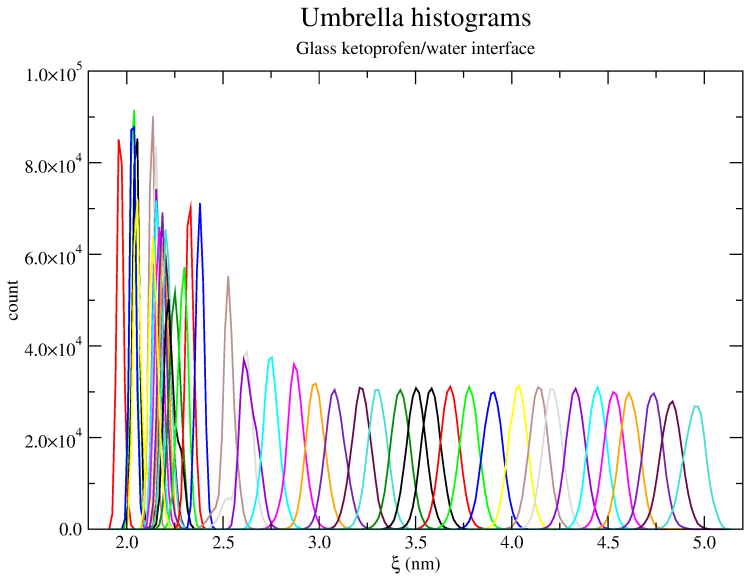

FIG. S3: Overlap of histograms used to reconstruct the free energy profile (see text) in the a-KTP case

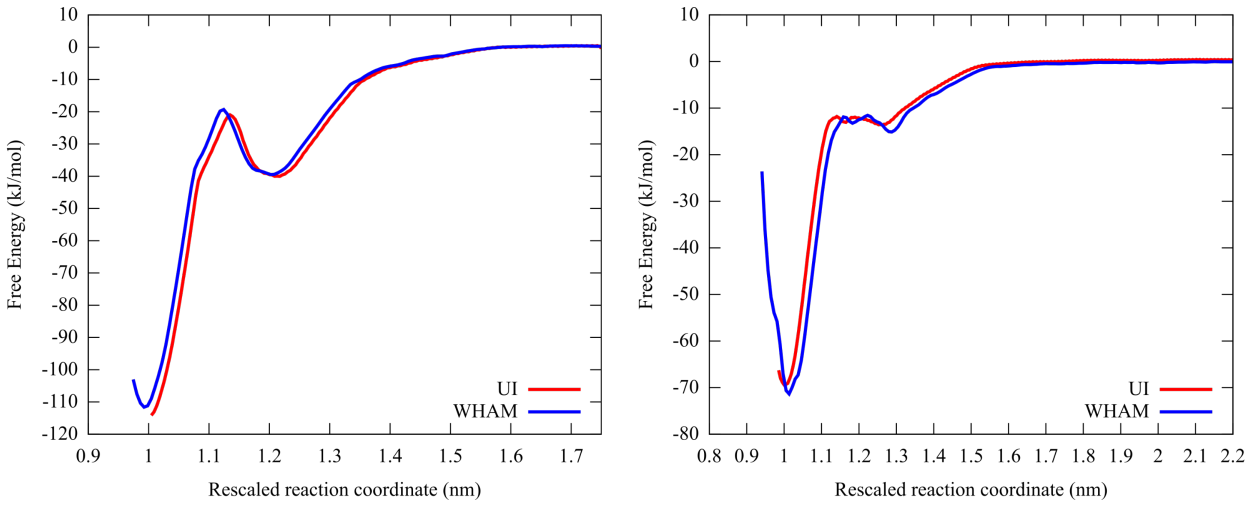

FIG. S4: Overlay of the free energy profiles of the dissolution of one KTP molecule from the crystal (left) and glass (right) solid states computed by WHAM (blue) and by the umbrella integration, UI, (red) method.

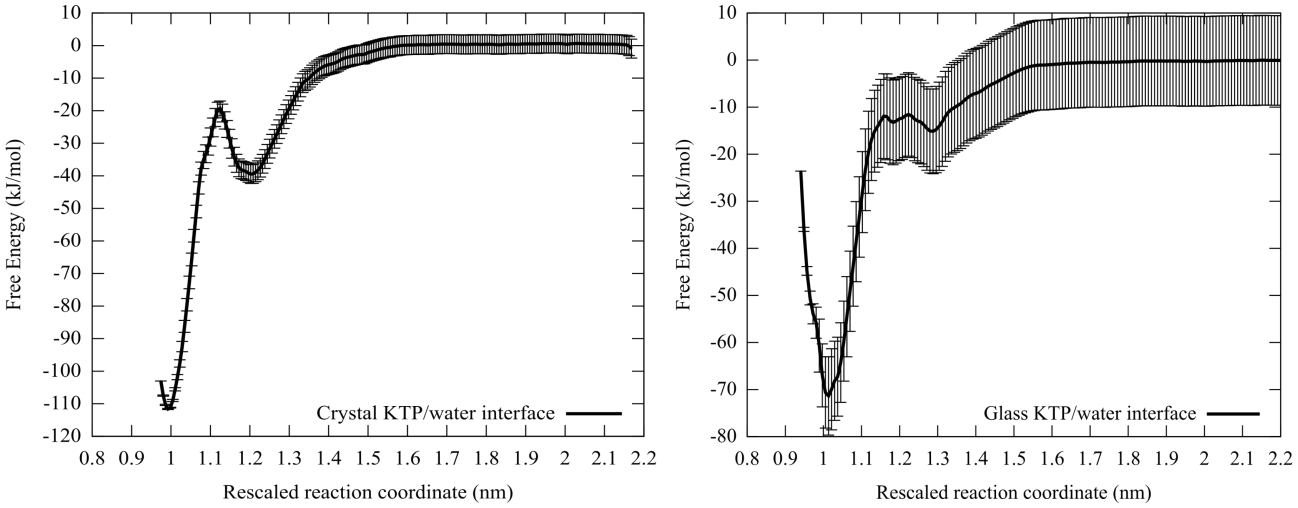

FIG. S5: Free energy profiles of the dissolution in water of one KTP molecule from the crystal (left) and amorphous (right) solid phases computed by WHAM. The statistical errors are estimated by the bootstrap analysis implemented in GROMACS considering the complete histograms as independent data points.

D. DFT computations

As stated in the main text, the DFT computations have been carried out using the CPMD[14] package based on pseudopotentials and plane waves. The PBE approximation[15] has been used, together with soft-norm conserving pseudopotentials[16] with a kinetic energy cutoff of 120 Ry. Periodic boundary conditions have been used, and the long range Coulomb interactions are computed using Ewald sums. Geometries are optimised by quenched MD. Dispersion energy is included using the semi-empirical approach of Grimme.[17] The vibrational analysis is carried out computing the dynamical matrix by finite differences, using the same setup of the QH approximation.

II. RESULTS OF DENSITY FUNCTIONAL COMPUTATIONS

A preliminary stage of validation of our methods has been carried out by comparing properties computed by density functional approximations (DFT) and by the force field among themselves and, whenever possible, with the results of experimental measurements. The details of the two simulation methods are reported in the main text and in Sec. I of these SI.

A. Comparison of the experimental and DFT crystal structure

The first comparison concerns the structure of the crystal measured by X-ray diffraction and computed by DFT at the experimental lattice parameters (Briard and Rossi, 1990), starting from the atomic coordinates given in Ref. 61 of the main text. The simulated sample consists of a single unit of two Ketoprofen molecules and 66 atoms (38 non-hydrogen atoms), of $P_{\bar{1}}$ (triclinic) symmetry and periodicity. The lattice parameters are listed in Table II of the main text. Minimisation of the energy with respect to the atomic coordinates has been achieved using quenched MD, as specified in the Method section.

The structure **optimised by DFT** is very close to the experimental one, having a square deviation per atom, χ^2, defined as:

$$\chi^2 = \sum_i^n \frac{\mid \mathbf{r}_i^{out} - \mathbf{r}_i^{in} \mid^2}{n} \tag{2}$$

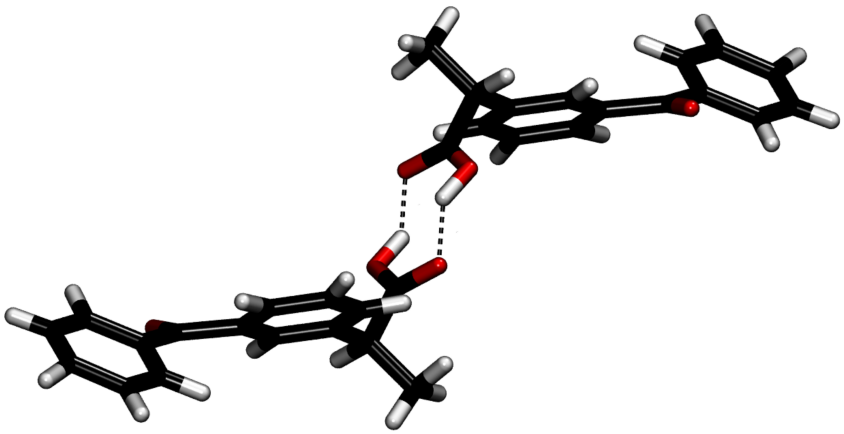

FIG. S6: Intermolecular hydrogen bonds formed by the hydroxyl moiety of the carbonyl group of two ketoprofen molecules located in adjacent cells. Experimental structure from Ref. 18.

equal to 0.04 Å ^{2} when the sum runs on the non-hydrogen atoms, and 0.067 Å ^{2} when the sum covers all atoms. As expected, the deviation is higher for hydrogen atoms, whose position is rather uncertain in X-ray diffraction measurements. To be precise, the structure reported in the experimental paper had one H atom less than the stoichiometric definition, which has been added to our input by standard software tools. The tighter identification of H atoms by DFT is reflected in the better definition of the pair of H-bonds at the carboxylic junction between two molecules, which appears stronger and more planar in the computational ground state structure (See Fig. S6) than in the experimental one. In the crystal structure, the carbonyl group at the center of the molecules does not accept a proper hydrogen bond, but nevertheless it forms weak hydrogen bonds with hydrogens belonging to aromatic rings.

Vibrational frequencies have been computed by diagonalising the dynamical matrix (i.e. the Hessian matrix weighted by the atomic masses) computed by finite difference. Only phonons at the Γ-point of the Brillouin zone of c-KTP has been considered.

Comparison of the ground state geometry shows that the experimental structure is fairly well reproduced also **by the force field**, having a mean square deviation (per atom), χ^2, equal to 0.11 Å ^{2} when considering non- hydrogen atoms, and 0.47 Å ^{2} when considering

all atoms. Visual inspection of the structure shows that the nearly perfect planarity of the phenyl rings displayed the experimental structure is reproduced by the force field. As expected, discrepancies are observed in the dihedral angles.

The good agreement of structural properties is reflected into the fair agreement of the vibrational density of states (vDOS). The comparison of the vDOS computed by DFT and by the force field is shown in Fig. S7.

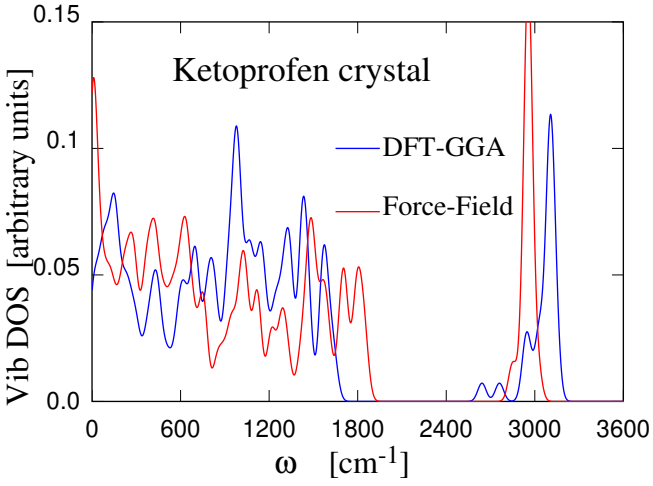

FIG. S7: Comparison of the vibrational density of states of crystalline ketoprofen computed by density functional computations (CPMD package) and by the GAFF force field.

The similarity of the two vDOS underlies the fair agreement of the vibrational contribution to the free energy per molecule shown in Fig. S8. Although the difference is quantitatively non-negligible at $T = 300$ K, this is due to differences in the intra-molecular frequencies, which largely cancel in the comparison of free energies among systems having the same number of molecules.

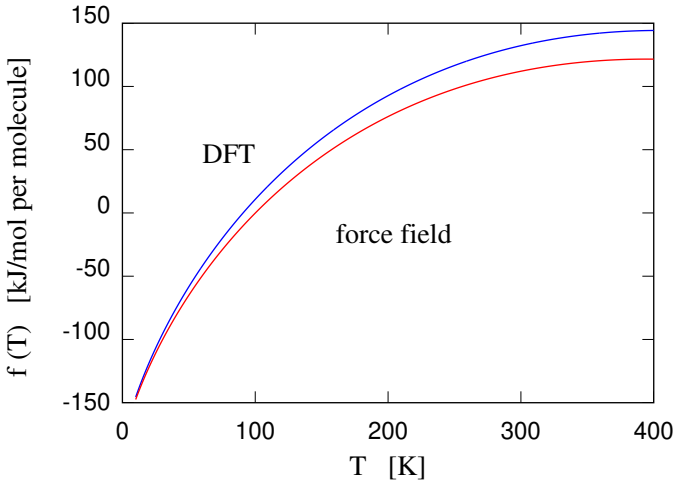

FIG. S8: Comparison of the harmonic free energy of c-KTP computed from the results of Fig. S7.

A limited comparison of DFT vibrational properties is possible also with experimental data, represented by infrared (FTIR) and Raman spectra.

In particular, a semiquantitative comparison with the data of Vueba et al., Int. J. Pharm. **2006**, *307*, 56-65 is possible for the high frequency modes, considering the experimental spectra for liquid and amorphous KTP, together with the DFT results for both crystal and gas phase KTP.

First of all, the frequency range $2600 \leq \omega \leq 3200$ cm^{-1} attributed to OH and CH stretching compares well with the corresponding range of stretchings found by DFT.

The highest frequency modes (3200 cm^{-1}) attributed to OH stretching only slightly affected by H-bonding can be found at a comparable frequency in the DFT results for the gas-phase molecule. The lowest frequency modes (2600 cm^{-1}) not unambiguously identified in the experimental paper, in DFT appear as OH stretching affected by strong H-bonding in the crystal.

The narrow band at $\omega \sim 1600 - 1700$ cm^{-1}, present both in the Raman spectra and in the DFT data, is due to the C=O stretching.

The lowest frequency modes are difficult to identify unambiguously.

For this reason, little comparison is possible with the data of Shibata et al., J. Mol. Struct. **2014**, *1062*, 185-188, whose data cover the range $0 \leq \omega \leq 250$ cm^{-1} only, although

the determination of the glass transition temperature $T_g = 267$ K they provide agrees closely with the computational (FF) result (see main text and Sec. III in SI).

As a further test of structural properties, the ground state geometry of a single (gas-phase) molecule has been determined by DFT and by the FF. The χ^2, in this case, turns out to be 0.06 Å ^{2} for non hydrogen atoms, and 0.10 Å ^{2} for all atoms.

A visual impression of the degree of agreement/disagreement is provided by Fig. S9, in which the DFT and FF ground state geometries have been superimposed.

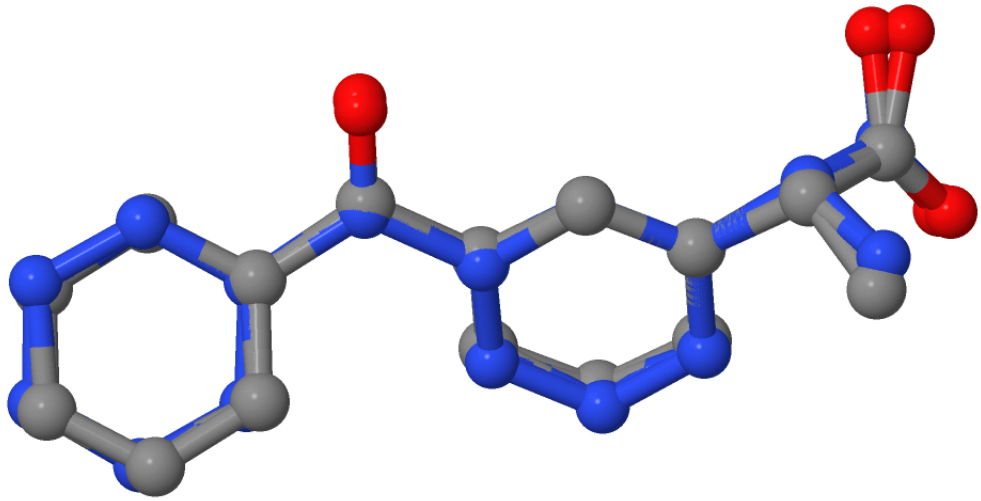

FIG. S9: Comparison of the ground state structure of a single (gas-phase) KTP molecule computed by DFT and by the GAFF FF. Carbon atoms in the FF structure are painted blue. Hydrogen atoms have been removed for the sake of clarity.

An important issue, relevant for the structure and cohesion of the amorphous phase concerns the relative stability of the *cis* and *trans* conformers of the gas phase KTP molecule. The results of DFT computations are summarised in Fig. S10.

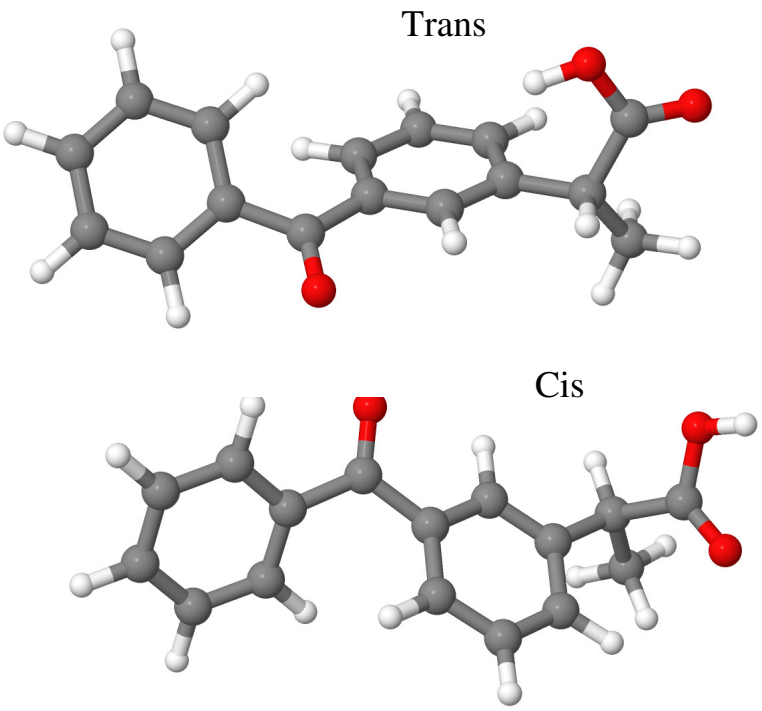

FIG. S10: Cis and Trans configurations determined by density functional computations (see text). The potential energy of the Trans configuration is $\Delta E = 12$ kJ/mol higher than that of the Cis configuration. Zero-point energy decreases this difference by 1.3 kJ/mol.

The result for the energy difference agrees qualitatively with that of M. L. Vueba, *et al.*, Int. J. Pharm. **2006**, *307*, 56, but differs in the quantitative estimate of ΔE, found to be 18.8 kJ/mol in the cited reference.

The corresponding value for the *cis-trans* energy difference computed by the force field is 8.6 kJ/mol.

III. SIZE DEPENDENCE OF THE KTP CRYSTAL FREE ENERGY

As stated in the main text (Sect. IIIC) the equilibrium volume of the KTP crystal at $T = 300$ K has been evaluated by QH computations on a sample of 36 molecules obtained by replicating $2 \times 3 \times 3$ times the experimental unit cell along the **a**, **b** and **c** lattice directions, respectively.

The value of the QH free energy, however, has been corrected for finite size effects, since test computations whose results are reported here, have shown a size dependence larger than in the amorphous samples.

To quantify finite size effects, two larger simulation cells have been considered, corresponding to $2\times3\times4$ and $2\times4\times4$ replicas, again along the **a**, **b** and **c** directions, respectively. The $2 \times 3 \times 4$ cell contains 48 KTP molecules and covers a volume of 12233.7 Å ^{3}. The $2\times4\times4$ cell is also the most isotropic one, it contains 64 molecules and has a volume 21756.7 Å ^{3}. The QH free energy per molecule at $T = 300$ K turns out to be $F_{QH}(300K) = 126.09$ kJ/mol and 125.39 kJ/mol for the two system sizes, respectively. The size dependence of the free energy is not completely negligible, and is likely to be due to the strict discretisation of phonon wave vectors in the crystal phase. This interpretation is confirmed by the observation that the potential energy per molecule at $T = 0$ K is virtually the same in the 36, 48 ad 64 molecule samples. Nevertheless, the free energy $F_{QH}(300) = 125.39$ kJ/mol per molecule of the largest and most isotropic system is our best approximation of the result in the thermodynamic limit, and in what follows it represents our reference free energy for c-KTP, as reported in Tab. 3 of the main text.

IV. PREPARATION AND PROPERTIES OF THE A-KTP SAMPLE

The preparation of the amorphous KTP sample has been carried out on a system made of 27 molecules in a cubic box. At first the sample has been equilibrated at $T = 460$ K during 200 ps. The system appears to be liquid with molecules diffusing through the sample volume. The temperature has been progressively reduced to 80 K at constant volume by decreasing the reference temperature of the Langevin thermostat according to a linear law, at a constant rate $\kappa = 1.44 \times 10^{11}$ K/s. The extreme cooling rate imposed by the short time scale of MD is several orders of magnitude faster than any process achievable in practice. Nevertheless, the glass temperature $T_g = 272$ K determined for the model (see Fig. S11) is in excellent agreement with the experimental estimate of $T_g = 267$ K.[19] Other experimental papers[20–23] provide T_g values that differ from $T_g = 267$ K by a few K at most.

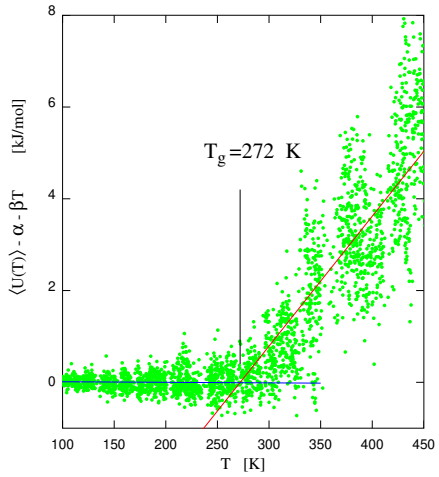

FIG. S11: Average potential energy $\langle U \rangle$ as a function of temperature during cooling of a KTP sample from the liquid phase. The glass transition temperature T_g is identified by the intersection of the two linear curves fitting the potential energy as a function of the temperature related to the liquid and glass phases, i.e. higher and lower temperatures, respectively. The plot reports the difference between the computed average potential energy and its interpolation at low temperature.

Structural and vibrational details identified in the simulated system are supported by experimental data. For instance, the pair of nearly parallel H-bonds that identify dimers in the crystal structure, play a much lesser role in the computational amorphous sample,

a feature confirmed by the structural data of Ref. 24 and by the vibrational spectroscopy data of Ref. 25. For instance, in our simulations at $T = 300$ K, each molecule on average accepts and donates 0.64 H-bonds, compared to the nearly one H-bond per molecules in the crystal phase at the same temperature (the pair of H-bonds in the dimers are shared by two molecules). Perhaps more importantly, the H-bonds in the amorphous phase do not lock pair of molecules into dimers, but link molecules into chains connected by H-bonds.[26,27] A crucial molecular isomerisation accompanies this structural transformation: while in a-KTP all molecules are *cis* with respect to the carbonyl group, in the liquid and in the amorphous state the *trans* conformer is more common.

To verify that the molecular mobility is still negligible at room temperature, we computed the time dependence of the mean square displacement per atom of a-KTP at $T = 300$ K. The results are shown in Fig. S12. Despite the temperature being ~ 30 K above T_g, the linear fit of the displacement as a function of time for $t \geq 100$ ps does not provide any estimate of non-vanishing diffusion outside the error bar.

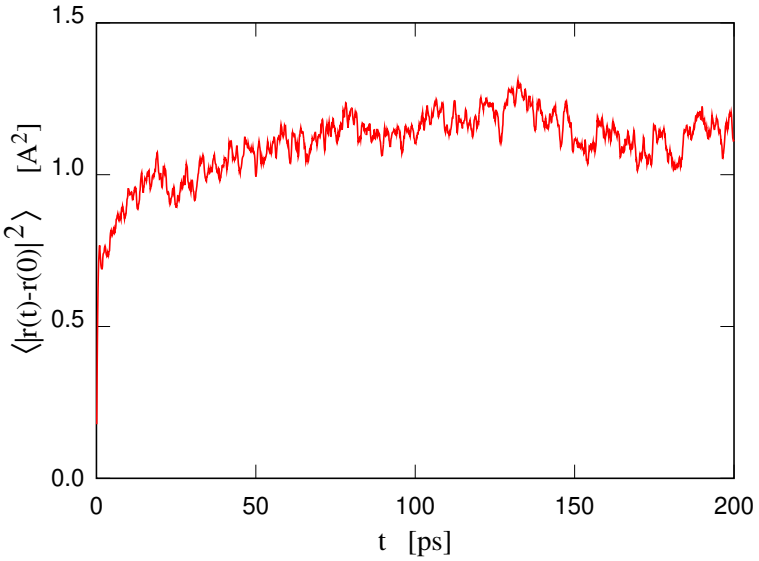

FIG. S12: Mean square displacement per atom in ketoprofen at $T = 300$ K.

V. THE VAPOUR PRESSURE OF KETOPROFEN IN EQUILIBRIUM WITH THE CRYSTAL AT $T = 300$ K

As an independent check of the validity of our method to compute solubility, we estimated the vapour tension of ketoprofen at $T = 300$ K in equilibrium with the crystal phase. The test is relevant because this quantity is available from experiments, but also because different approaches to compute solubility combine independent estimates of the free energy change in moving one crystal molecule first to the vapour phase (sublimation free energy) and then to the solvated state (solvation free energy).

In our study, the computation of the KTP free energy in the vapour phase has been computed in full analogy with the computation of absolute free energies described in the main text, i.e., i) relaxing a single molecule to its minimum energy structure; ii) computing the harmonic free energy as a function of temperature; iii) estimating the anharmonic contributions by λ-integration at $T_{low} = 100$ K, extended to $T = 300$ K by integration over β.

The harmonic free energy of the KTP molecule is $F_h(300K) = 250.22$ kJ/mol, while its classical rotational free energy, computed from the principal momenta di inertia of the molecular ground state geometry, is $\Delta F_{rot} = -38.70$ kJ/mol. Integration over λ at $T = 100$ K and over β, carried out at fixed centre of mass and vanishing angular momentum, gives $\Delta F_{\lambda} = -1.85$ kJ/mol and $\Delta F_{\beta}^{exc} = -0.39$ kJ/mol.

Combining these data with the free energy of the crystal, one obtains:

$$k_B T \log \frac{\rho_v}{\rho_s} = -83.01 \qquad kJ/mol \tag{3}$$

where ρ_v and ρ_s are the densities of the vapour and of the crystal phase, respectively. This one is computed from the equilibrium volume per molecule estimated in Sec. IIIC of the main text, giving $\rho_v(300K) = 1.12\ 10^7$ cm^{-3}. At this low density, the system is an ideal gas and the pressure is computed as:

$$P = \rho_v k_B T = 4.93\ 10^{-7} \qquad Pa \tag{4}$$

or $P = 4.93\ 10^{-12}$ atm. The agreement with the experimental data ($P = 1.05\ 10^{-10}$ atm, see Ref. 28) is qualitatively acceptable, but certainly not quantitatively accurate. The better agreement for the solubility of KTP in water is likely to be due to enhanced compensation of

errors in comparing condensed phases (KTP/water, water and KTP crystal) of comparable density. The larger error for the vapour phase might in fact be due to a residual density dependence of the force field, optimised on condensed phases. Nevertheless, the computational estimate of the sublimation free energy is still within 7.6 kJ/mol, or less than 2 kcal/mol from the experimental value.

By construction, the λ and β integrations for the isolated molecule are not affected by translations and rotations, hence the anharmonic contribution at $T = 300$ K can be reliably computed directly at $T = 300$ K by λ-integration only. The result of this exercise ($\Delta F_\lambda = -2.46 \equiv \Delta F$ kJ/mol) is fully compatible with the result of the previous estimate ($\Delta F = -2.24$ kJ/mol), supporting the validity of our approach splitting the estimate of $\Delta F(300K)$ into separate perturbation steps.

The free energy of the gas-phase molecule computed in this Section can be combined with those for water and KTP in water to compute the solvation free energy, i.e., the transfer free energy per molecule ΔF_{gw} from the ideal gas phase to the water solution. This last comparison gives $\Delta F_{gw} = -56.46$ kJ/mol, in good agreement with the experimental result.[29] It is apparent that the error in the gas phase free energy is partly compensated by the error in the solvation free energy (4.8 kJ/mol), to give a fair solubility whose corresponding free energy error is only 2.8 kJ/mol. In comparing with previously published results, one should take into account that our data concern transfer free energies among systems in equilibrium with each other, while several published papers consider the vapour and the solution at standard conditions (unit concentration) not corresponding to mutual equilibrium.

VI. THE MASS DENSITY PROFILE AT THE C-KTP/WATER AND A-KTP/WATER INTERFACE

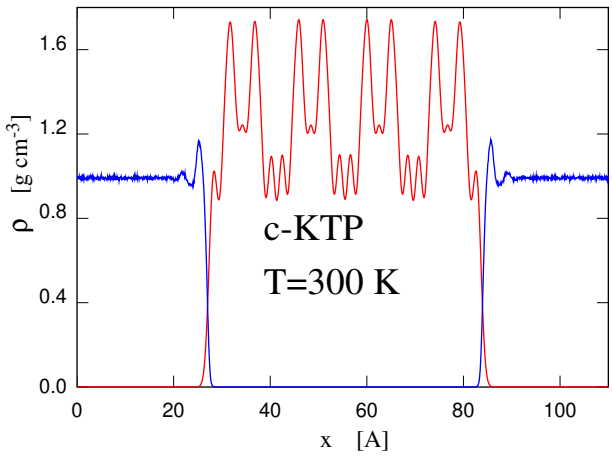

FIG. S13: Mass density profile at the c-KTP/water interface. Red line: KTP atoms. Blue line: water atoms.

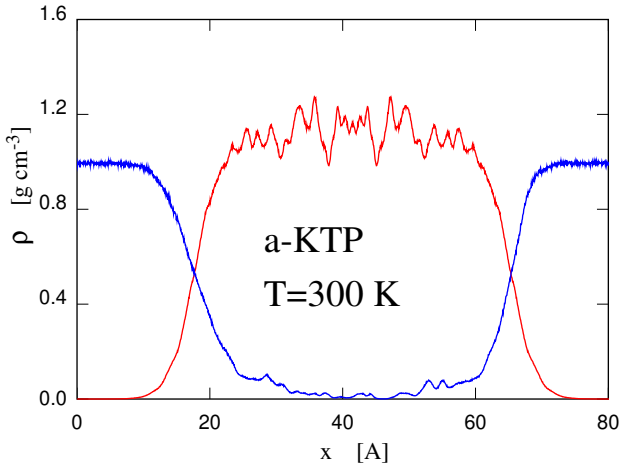

FIG. S14: Mass density profile at the a-KTP/water interface. Red line: KTP atoms. Blue line: water atoms. The a-KTP/water interface is much broader than the c-KTP/water interface shown in Fig. S13.

VII. WATER SORPTION IN A-KTP

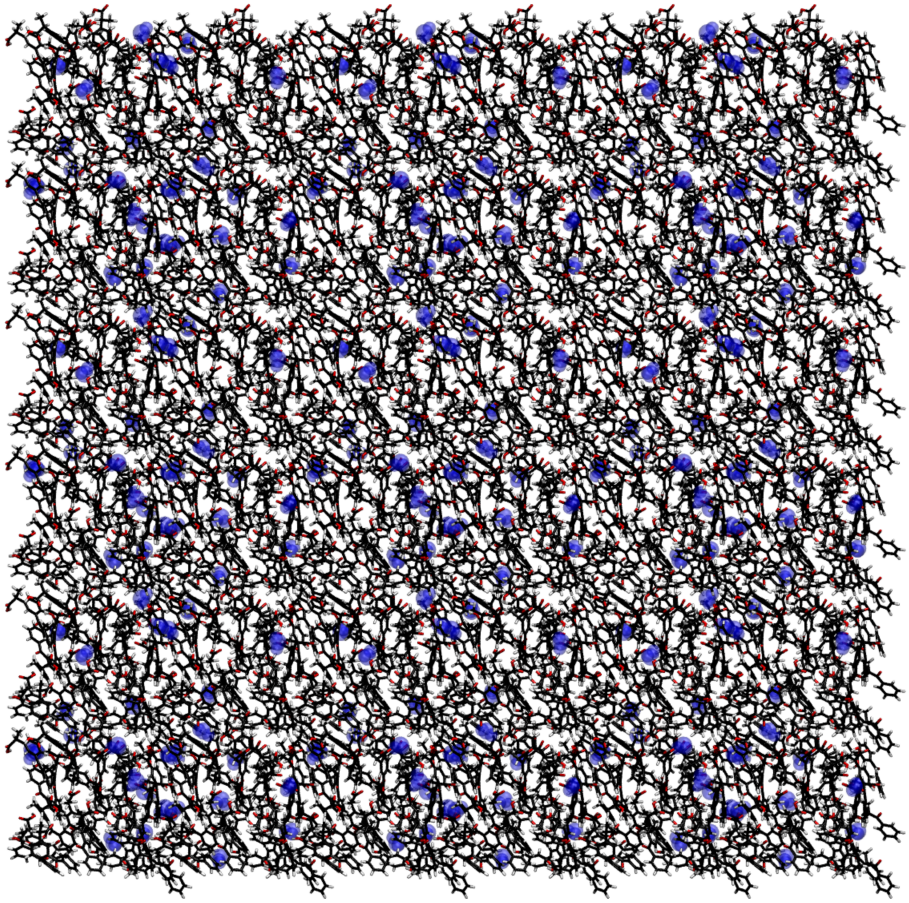

FIG. S15: Distribution of water molecules in nanocavities found by the *solvate* tool of Gromacs

[1] Wang, J.; Wolf, R. M.; Caldwell, J. W.; Kollman, P. A.; Case, D. A. Development and testing of a general Amber force field. *J. Comput. Chem.* **2004**, *25*, 1157-1174.

[2] Wu, Y.; Tepper, H. L.; Voth, G. A. Flexible simple point-charge water model with improved liquid-state properties. *J. Chem. Phys.* **2006**, *124*, 024503.

[3] Grønbech-Jensen, N.; Farago, O. A simple and effective Verlet-type algorithm for simulating Langevin dynamics. *Mol. Phys.* **2013**, *111*, 983-991.

[4] Birch, F. Finite elastic strain of cubic crystals. *Phys. Rev.* **1947**, *71*, 809-824.

[5] Abraham, M. J.; Murtola, T.; Schulz, R.; Páll, S.; Smith, J. C.; Hess, B.; Lindahl, E., GROMACS: High performance molecular simulations through multi-level parallelism from laptops to supercomputers. *SoftwareX* **2015**, *1-2*, 19-25.

[6] Páll, S.; Hess, B., A flexible algorithm for calculating pair interactions on SIMD architectures. *Comp. Phys. Comm.* **2013**, *184*, 2641-2650.

[7] Darden, T.; York, D.; Pedersen, L., Particle mesh Ewald: An $N \log(N)$ method for Ewald sums in large systems. *J. Chem. Phys.* **1993**, *98*, 10089-10092.

[8] Parrinello, M.; Rahman, A., Polymorphic transitions in single crystals: A new molecular dynamics method. *J. Appl. Phys.* **1981**, *52*, 7182-7190.

[9] Park, S.; Schulten, K., Calculating potentials of mean force from steered molecular dynamics simulations. *J. Chem. Phys.* **2004**, *120*, 5946-5961.

[10] Kumar, S.; Rosenberg, J. M.; Bouzida, D.; Swendsen, R. H.; Kollman, P. A. The weighted histogram analysis method for free-energy calculations on biomolecules. I. The method. *J. Comput. Chem. 1992*, *13*, 1011-1021.

[11] GitHub project ATB-UQ/umbrella_integration, DOI: 10.5281/zenodo.164996

[12] Kaestner, J.; Thiel, W. Bridging the gap between thermodynamic integration and umbrella sampling provides a novel analysis method: "Umbrella integration". *J. Chem. Phys.* **2005**, *123*, 144104.

[13] Kaestner, J., Thiel, W. Analysis of the statistical error in umbrella sampling simulations by umbrella integration. *J. Chem. Phys.* **2006**, *124*, 234106.

[14] CPMD http://www.cpmd.org/, Copyright IBM Corp 1990-2019, Copyright MPI für Festkörperforschung Stuttgart 1997-2001.

[15] Perdew, J. P.; Burke, K.; Ernzerhof, M. Generalized gradient approximation made simple. *Phys. Rev. Lett.* **1996**, *77*, 3865-3868.

[16] Troullier, N.; Martins, J. L. Efficient pseudopotentials for plane-wave calculations. *Phys. Rev. B* **1991**, *43*, 1993-2006.

[17] Grimme, S. Semiempirical GGA-type density functional constructed with a long-range dispersion correction. *J. Comp. Chem.* **2006**, *27*, 1787-1789.

[18] Briard, P.; Rossi, J. C. Kétoprofène. *Acta Cryst. C* **1990**, *46*, 1036-1038.

[19] Sailaja, U.; Shahin Thayyil, M.; Krishna Kumar, N. S.; Govindaraj, G. Molecular dynamics in liquid and glassy states of non-steroidal anti-inflammatory drug: ketoprofen. *Eur. J. Pharm. Sci.* **2013**, *49*, 333-340.

[20] Baird, J. A.; Van Eerdenbrugh, B.; Taylor, L. S. A classification system to assess the crystallization tendency of organic molecules from undercooled melts. *J. Pharm. Sci.* **2010**, *99*, 3787-3806.

[21] Pajula, K.; Taskinen, M.; Lehto, V. P.; Ketolainen, J.; Korhonen, O. Predicting the formation and stability of amorphous small molecule binary mixtures from computationally determined Flory-Huggins interaction parameter and phase diagram. *Mol. Pharm.* **2010**, *7*, 795-804.

[22] Di Martino, P.; Joiris, E.; Gobetto, R.; Masic, A.; Palmieri, G. F.; Martelli, S. Ketoprofen-poly(vinylpyrrolidone) physical interaction. *J. Cryst. Growth.* **2004**, *265*, 302-308.

[23] Shibata, T.; Takayama, H.; Kim, T. H.; Kojima, S. Acoustic and thermal anomalies in a liquid-glass transition of racemic S(+)-R(-) ketoprofen. *Chem. Phys. Lett.* **2014**, *592*, 80-84.

[24] Ottou Abe, M. T.; Correia, N. T.; Ndjaka, J. M. B.; Affouard, F. A comparative study of ibuprofen and ketoprofen glass-forming liquids by molecular dynamics simulations. *J. Chem. Phys.* **2015**, *143*, 164506.

[25] Shibata, T.; Igawa, H.; Kim, T. H.; Mori, T.; Kojima, S. Glass transition dynamics of anti-inflammatory ketoprofen studied by Raman scattering and terahertz time-domain spectroscopy. *J. Mol. Structure* **2014**, *1062*, 185-188.

[26] Abe, M. T. O.; Correia, N. T.; Valdes, L.-C.; Ndjaka, J. M. B.; Affouard, F. Local molecular organizations of ibuprofen, flurbiprofen and ketoprofen in the liquid phase: Insights from molecular dynamics simulations. *J. Mol. Liq.* **2015**, *205*, 74-77.

[27] Abe, M. T. O.; Correia, N. T.; Ndjaka, J. M. B.; Affouard, F. A comparative study of ibuprofen and ketoprofen glass-forming liquids by molecular dynamics simulations. *J. Chem.Phys.* **2015**, *143*, 164506.

[28] Perlovich, G. L.; Kurkov, S. V.; Kinchin, A. N.; Bauer-Brandl A. Thermodynamics of solutions IV: Solvation of ketoprofen in comparison with other NSAIDs. *J. Pharm. Sci.* **2003** *92*, 2502-2511.

[29] Avdeef, A. Solubility of sparingly-soluble ionizable drugs. *Adv. Drug Deliv. Rev.* **2007**, *59*, 568-590.